Innovation Series https://www.innoseries.com

Numerical Assessment of Spoiler Angle Effects on Aerodynamic Performance of the Sedan Cars Using Computational Fluid Dynamics

Hanyun Yang
Beijing City International School, Beijing, China

Abstract: Optimizing aerodynamic design has become a key focus in automotive engineering as it plays a crucial role in improving fuel efficiency. This study employs the Computational Fluid Dynamics (CFD) method to investigate the effect of spoiler angles on the drag and lift coefficient of a sedan car for optimal performance. Airflow field information including pressure, velocity and turbulent kinetic energy around the car body is carefully visualized and analyzed. The drag and lift coefficients are quantified across different spoiler angles, revealing their effects on aerodynamic performance. Quantitative analysis shows that the drag coefficient increased by up to 178.6%, while the lift coefficient improved (became more negative) by 245.2% across the tested angles. A spoiler angle of 15° to 25° is expected to provide the most effective trade-off as it offers significant downforce enhancement with a relatively moderate increase in drag. These findings are expected to offer insights for designing spoilers that enhance vehicle efficiency, stability, and overall performance.

Keywords: CFD; Car; Aerodynamics; Drag and Lift Coefficient; Fuel Saving

1. Introduction

In recent years, the rapid growth of global transportation has led to a significant increase in energy consumption and carbon emissions. According to recent statistics, the transportation sector accounts for nearly 25% of global CO2 emissions, with passenger vehicles being one of the largest contributors [1-5]. As fuel prices continue to rise and environmental concerns grow, improving energy efficiency in vehicles has become a critical focus for both manufacturers and consumers. Therefore, developing sustainable transportation is crucial in the field of automobiles.

To address these challenges, the automotive industry has been exploring various solutions, including the development of electric vehicles (EVs) and the optimization of aerodynamic designs. Aerodynamic efficiency, influenced by factors like body shape, underbody design, wheel geometry, and rear spoiler configuration, plays a pivotal role in minimizing air resistance—a major source of energy loss at high speeds. Even marginal improvements in a vehicle's drag coefficient can yield substantial fuel savings; for instance, reducing Cd by 10% enhances fuel efficiency by approximately 5–7% under typical driving conditions [6]. Among these components, spoilers are particularly critical for balancing lift reduction and drag minimization. Spoilers are designed to manipulate the airflow around a vehicle, reducing lift and potentially decreasing drag. However, the effectiveness of a spoiler is highly dependent on its design, with the angle of the spoiler being a particularly critical parameter [7-9]. Different spoiler angles can lead to vastly different fluid flow patterns around the car, which in turn affects the airflow distribution on the vehicle's body.

Historically, wind tunnel testing dominated aerodynamic research, enabling precise physical measurements of airflow behavior. However, despite its accuracy, this method is prohibitively expensive and time-consuming, limiting iterative design exploration. Alternatively, the Computational Fluid Dynamics (CFD) method now offers a cost-effective design solution. CFD enables detailed simulations of fluid flow around virtual models, allowing engineers to test multiple configurations efficiently. Previous studies, (Deng et al. (2020), highlight the role of spoilers in managing airflow separation and pressure distribution. Building on this foundation, this study employs CFD to evaluate how varying spoiler angles affect the Toyota GT86's drag coefficient, aiming to identify design guidelines for improved aerodynamic performance.

In this study, a 3D car model based on the Toyota GT86 prototype was first numerically built, followed by the addition of a spoiler with angles of 15°, 25°, and 35°, respectively. The aerodynamic performance of the aforementioned models was tested by intuitively visualizing their velocity, pressure, and turbulent kinetic energy. The lift and drag coefficients were subsequently analyzed.

2. Methods

2.1 Computational Domain and Boundary Conditions

In this study, the baseline car model based on the Toyota GT86 was first numerically built using SolidWorks 2022. Three spoilers with varying angles, i.e., 15°, 25°, and 35°, were subsequently added to the baseline model for further aerodynamic performance evaluation. To maintain consistency across configurations, the spoiler's position and chord length were kept constant. Non-essential components, including mirrors and wheels, were removed to reduce mesh complexity while retaining critical aerodynamic surfaces. The final model was imported into ANSYS CFX and placed within a far-field domain, as illustrated in Figure 1. A uniform velocity of 120 km/h (33.33 m/s) with a turbulence intensity of 5% and a turbulent viscosity ratio of 10 was applied to simulate highway airflow. The static pressure was set to 0 Pa (gauge) to represent atmospheric conditions, and a no-slip condition with smooth wall treatment was enforced for the stationary wall, approximating a fixed road surface. To optimize computational efficiency, a longitudinal symmetry plane was introduced to halve the computational costs while maintaining flow accuracy.

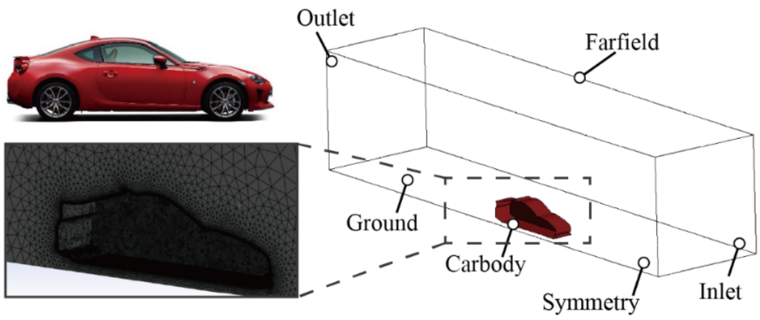

Figure 1: Computational Model of the Sedan Car (Toyota GT86) and Mesh Details.

A 3-dimensional model was discretized using unstructured tetrahedral mesh elements. A mesh independence study was first conducted with three different mesh configurations, ultimately selecting a configuration with 0.77 million elements. To accurately capture the detailed airflow variation in the near-wall region, 5 prism layers with a growth ratio of 1.2 were applied. The tested cases in this study are outlined in following Table 1.

Table 1: Summary of Case Studies.

	Spoiler Angles
Case 1	Without Spoiler
Case 2	15°
Case 3	25°
Case 4	35°

2.2 Mathematical Equations

The airflow in relation to temperature, velocity, pressure, and density was solved using the incompressible Navier-Stokes (N-S) equation [10]. The 3-dimensional continuity equation (eq.1) and momentum equation (eq.2) can be expressed as:

$$\frac{\partial u}{\partial x}+\frac{\partial v}{\partial y}+\frac{\partial w}{\partial z}=0 \tag{1}$$

$$\begin{gathered}
u\frac{\partial u}{\partial x}+v\frac{\partial u}{\partial y}+w\frac{\partial u}{\partial z}=-\frac{1}{\rho}\frac{\partial P}{\partial x}+v\left[\frac{\partial^2 u}{\partial x^2}+\frac{\partial^2 u}{\partial y^2}+\frac{\partial^2 u}{\partial z^2}\right]\\
u\frac{\partial v}{\partial x}+v\frac{\partial v}{\partial y}+w\frac{\partial v}{\partial z}=-\frac{1}{\rho}\frac{\partial P}{\partial y}+v\left[\frac{\partial^2 v}{\partial x^2}+\frac{\partial^2 v}{\partial y^2}+\frac{\partial^2 v}{\partial z^2}\right]\\
u\frac{\partial w}{\partial x}+v\frac{\partial w}{\partial y}+w\frac{\partial w}{\partial z}=-\frac{1}{\rho}\frac{\partial P}{\partial z}+v\left[\frac{\partial^2 w}{\partial x^2}+\frac{\partial^2 w}{\partial y^2}+\frac{\partial^2 w}{\partial z^2}\right]
\end{gathered} \tag{2}$$

where, P is the pressure, ρ is the density, v is the kinematic viscosity of fluid, u, v and w are the velocities in x, y and z directions respectively.

In this study, the turbulent flow characteristics were captured using the standard k-ε models which solves two additional transport equations for turbulent kinetic energy (k) and dissipation rate (ε) [11-13]:

$$\frac{\partial k}{\partial t}+\mathbf{U}\cdot\nabla k=\nabla\cdot(\nu_t\nabla k)+P_k-\epsilon \tag{3}$$

$$\frac{\partial \varepsilon}{\partial t}+\mathbf{U}\cdot\nabla\varepsilon=\nabla\cdot\left(\frac{\nu_t}{\sigma_\varepsilon}\nabla\varepsilon\right)+C_{1\varepsilon}\frac{\varepsilon}{k}P_k-C_{2\varepsilon}\frac{\varepsilon^2}{k} \tag{4}$$

where k is the turbulent kinetic energy, ϵ is the dissipation rate, ν_t is the turbulent viscosity, P_k is the production of turbulent kinetic energy, C_1 and C_2 are model constants, $\mathbf{U}$ is the velocity field, P is the pressure, ρ is the fluid density, ν is the kinematic viscosity of the fluid, and u, v, and w are the velocities in the x, y, and z directions, respectively.

3. Results and Discussion

Figure 2 illustrates the velocity pattern around the car body with and without the spoiler. For the baseline model (case 1), it can be observed that the stagnation point occurs at the front of the vehicle, where, according to Bernoulli's principle, the velocity is zero and the pressure is at its maximum. This high-pressure zone leads to a significant pressure drag, as the flow slows down sharply at the vehicle's front, causing the airflow to separate further downstream. Airflow separates abruptly at the trunk edge, creating a large low-velocity recirculation zone behind the vehicle. This leads to a high-pressure differential between the front stagnation point (with zero velocity and maximum pressure) and the low-pressure wake, increasing pressure drag. Further introducing the spoiler is found to significantly alter the flow dynamics at the rear of the vehicle. It changes the recirculation zone, increasing its size and expanding the wake region. This modification in the velocity pattern potentially increases drag, as the enlarged recirculation zone leads to higher turbulence and pressure drag at the rear of the vehicle.

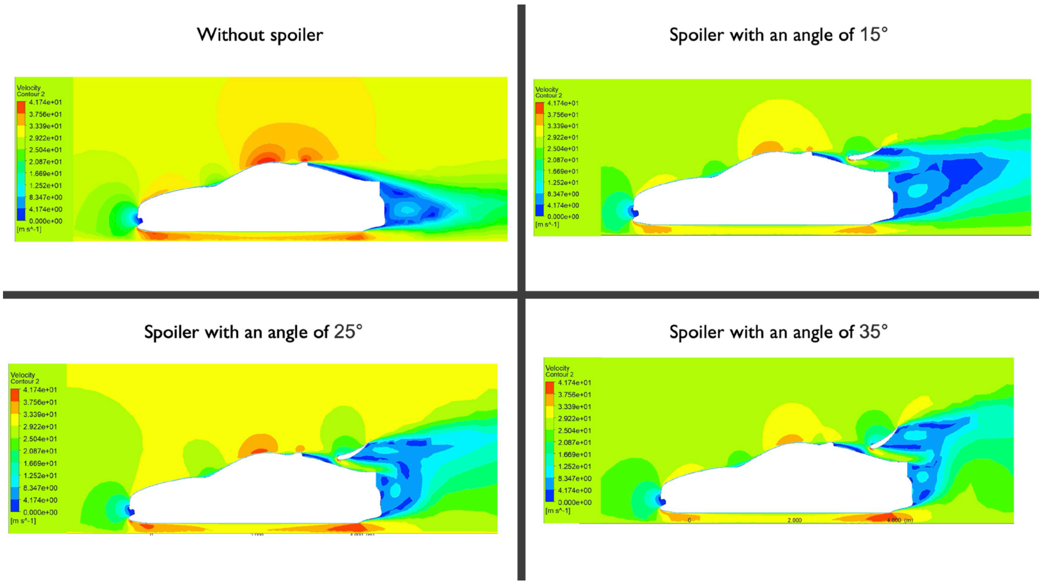

Figure 2: Velocity Pattern Around the Car Body.

Figure 3 reveals the pressure distribution pattern around the car body for different case scenarios. Without a spoiler, the front stagnation point shows consistently high pressure, in accordance with Bernoulli's principle, where zero velocity corresponds to maximum static pressure. In contrast, the rear of the vehicle exhibits a pronounced negative pressure zone, which is a result of flow separation and vortex shedding. Further introducing the spoiler, it can be observed that a new high-pressure region forms above the spoiler. This indicates that by adding the spoiler, the vehicle generates increased downforce, which enhances the car's grip on the road, improving stability and control.

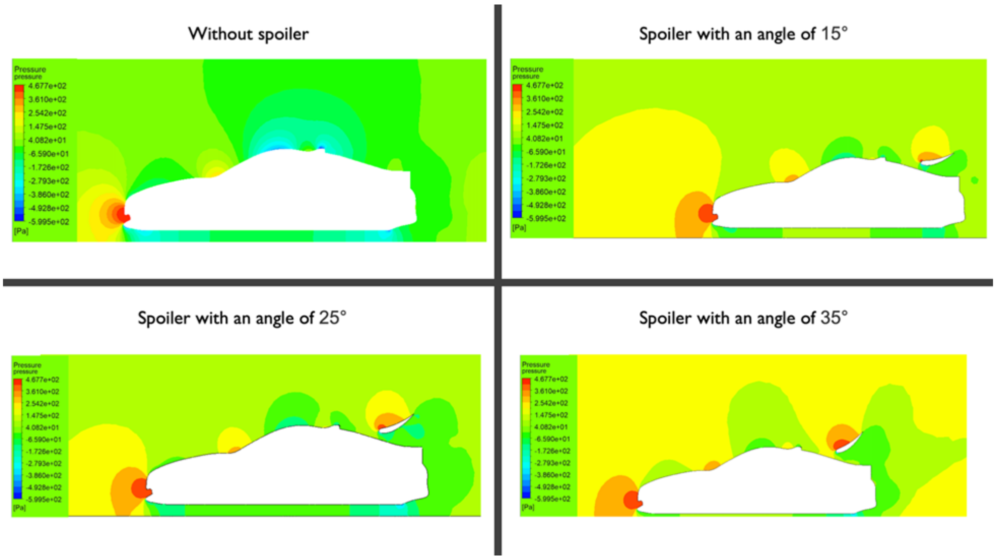

Figure 3: Pressure Distribution Around the Car Body.

Analysis of turbulence kinetic energy (TKE) (Figure 4) reveals how spoiler angles affect flow unsteadiness and, consequently, drag. Without a spoiler, the wake shows broad, high-TKE regions, primarily caused by vortex shedding and unsteady separation at the trunk edge. This pattern is indicative of turbulent dissipation in an unmanaged flow, leading to significant drag. When a spoiler is introduced, the turbulence structure at the rear of the vehicle changes. At a 15° angle, the turbulence region expands significantly, which potentially increases drag due to the larger wake and more intense turbulent dissipation. At 25° and 35° angles, the turbulence structure at the rear undergoes further changes. The turbulent wake near the vehicle merges with the spoiler-induced flow, leading to a more compact wake structure. This alteration in the wake shape generates additional downforce, especially at the higher angles, by stabilizing the rear flow. However, the increased downforce may come at the cost of increased drag, as the wake structure becomes more complex and the turbulent dissipation increases.

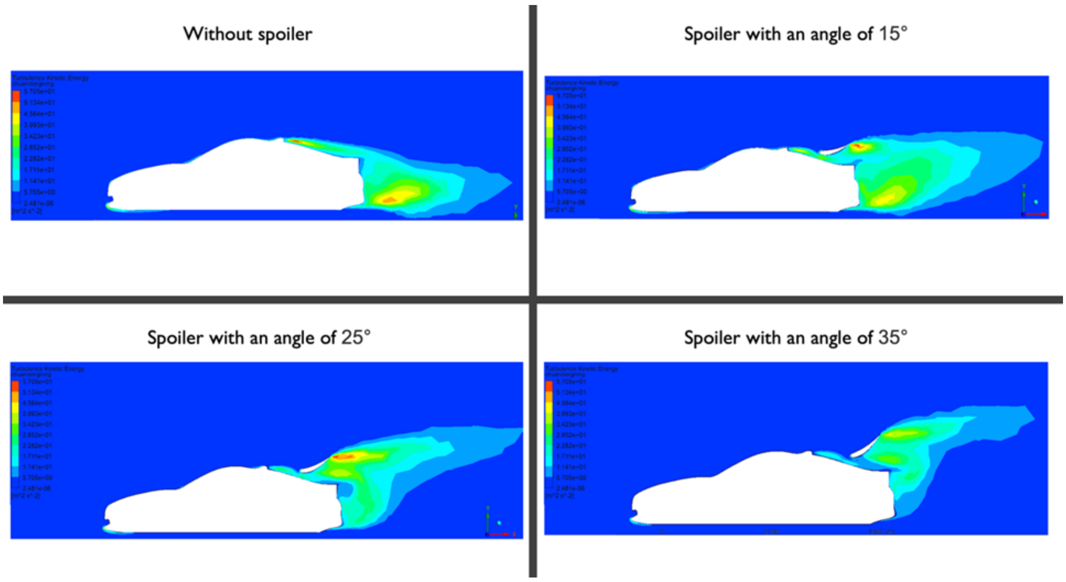

Figure 4: Turbulence Kinetic Energy Around the Car Body.

The aerodynamic performance was ultimately summarized using the drag and lift coefficient, as illustrated in Figure 5. Quantitatively, it is found that as the spoiler angle increases from 0° to 35°, the drag coefficient gradually rises, indicating higher aerodynamic resistance. Meanwhile, the lift coefficient becomes more negative, reflecting increased downforce. This suggests a clear trade-off: while larger spoiler angles enhance stability through greater downforce, they also lead to higher drag, potentially reducing overall efficiency. Quantitative results are further outlined in Table 2.

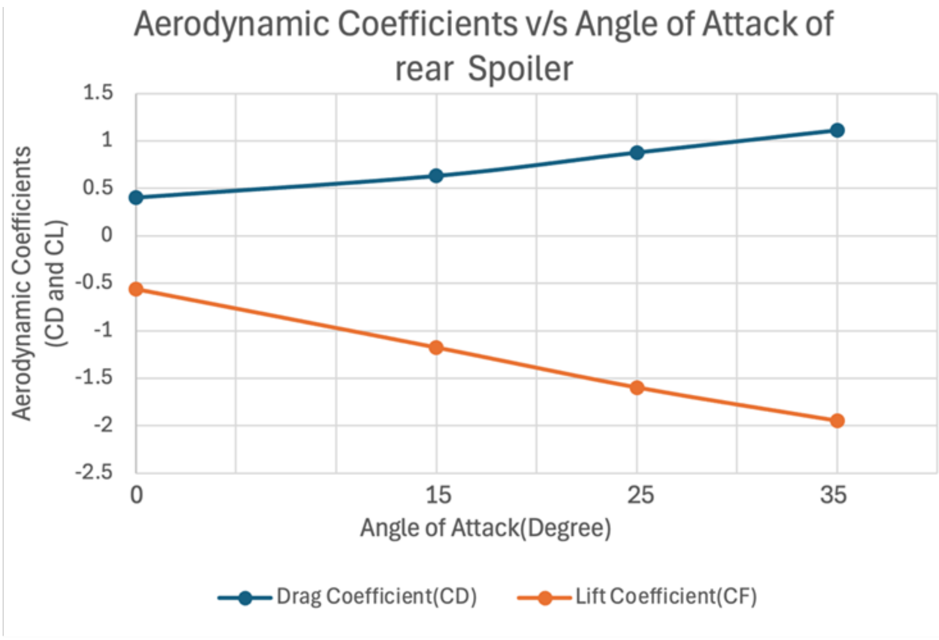

Figure 5: Drag and Lift Coefficient Comparison Among the Cases.

Table 2 displays the aerodynamic coefficients at different spoiler angles. In comparison to the baseline scenario without a spoiler, augmenting the spoiler angle to 15° leads to a 57.6% escalation in drag and a 108.7% rise in downforce (more negative lift coefficient). At 25°, the drag escalates by 119.5%, whereas the downforce amplifies by 183.1% relative to the baseline. Ultimately, at 35°, drag escalates by 178.6%, while downforce amplifies by 245.2%. Although downforce and drag both rise with spoiler angle, downforce enhancement initially occurs at a faster rate than drag, particularly between 0° and 25°. But after 25°, the drag penalty grows out of proportion to the downforce gain, indicating a decline in aerodynamic returns. Consequently, a more effective balance between increasing stability and reducing drag growth is achieved at moderate angles (about 15° to 25°).

Table 2: Aerodynamic Coefficients Across Spoiler Angles.

Spoiler Angle (°)	Drag Coefficient (Cd)	Lift Coefficient (Cl)
Without Spoiler	0.399951	-0.56407
15	0.630395	-1.17753
25	0.87777	-1.59669
35	1.11429	-1.94662

4. Conclusion

The results arising from the study revealed that the spoiler angle has a great impact on airflow behavior, pressure distribution, turbulence characteristics and the aerodynamic coefficient. Quantitative analysis shows that the drag coefficient increased by up to 178.6%, while the lift coefficient improved (became more negative) by 245.2% across the tested angles. A spoiler angle of 15° to 25° is expected to provide the most effective trade-off as it offers significant downforce enhancement with a relatively moderate increase in drag. These findings aimed to provide practical insights for car aerodynamic optimization using the CFD method.

References

[1] Granados-Ortiz F J, Morales-Higueras P, Ortega-Casanova J. 3D CFD simulation of the interaction between front wheels&brake ducts and optimised five-element F1 race car front wings under regulations. Alexandria engineering journal, 2023, 69: 677-698.

[2] Wang C, Wood J, Wang Y, et al. CO2 emission in transportation sector across 51 countries along the Belt and Road from 2000 to 2014. Journal of Cleaner Production, 2020, 266: 122000.

[3] Wang S, Ge M. Everything you need to know about the fastest-growing source of global emissions: Transport[J]. World Resources Institute, 2019, 16.

[4] Ritchie H. Cars, planes, trains: where do CO_2 emissions from transport come from? Our world in data, 2020.

[5] Tiseo I. Distribution of carbon dioxide emissions produced by the transportation sector worldwide in 2020, by subsector. Statista, 2023.

[6] Naidu S C V R M, Madhavan V M, Chinta S, et al. Analysis of aerodynamic characteristics of car diffuser for dissimilar diffuser angles on Sedan's using CFD. Materials Today: Proceedings, 2023, 92: 240-248.

[7] Selvam M A J, Kumar M R, Padmanabhan S, et al. Analyzing the downforce generated by rear spoiler of hatchback vehicle and creating an aeromapp using CFD analysis. Materials Today: Proceedings, 2023, 92: 48-55.

[8] Cheng S Y, Chin K Y, Mansor S, et al. Experimental study of yaw angle effect on the aerodynamic characteristics of a road vehicle fitted with a rear spoiler. Journal of Wind Engineering and Industrial Aerodynamics, 2019, 184: 305-312.

[9] Amer M, Yang C C, Chen H Y, et al. Experimental Investigation of a Spoiler's Impact on the Flow Pattern of a High-Speed Sport Car. Journal of Mining and Mechanical Engineering, 2020, 1(2): 73-84.

[10] Zaareer M N M, Mourad A H I, Darabseh T, et al. Impact of a vehicle exhaust pipe position on the lift and drag coefficients: 2D and 3D simulations. International Journal of Thermofluids, 2023, 18: 100321.

[11] Wang G, Yang F, Wu K, et al. Estimation of the dissipation rate of turbulent kinetic energy: A review. Chemical Engineering Science, 2021, 229: 116133.

[12] Lueck R. Calculating the rate of dissipation of turbulent kinetic energy. Rockland Scientific International Tech. Note TN-028, 2013, 18.

[13] Vassilicos J C. Dissipation in turbulent flows. Annual review of fluid mechanics, 2015, 47(1): 95-114.